Supporting Information

Centimeter-Sized Single Crystals of 2D Hybrid Perovskite toward Ultraviolet Photodetection with Anisotropic Photoresponse

Xinyi Niu,[a, b] Lishan Liang,[a, b] Xinyuan Zhang,[a] Ziyang Wang,[a] Tingting Zhu,[a] Jianbo Wu,[a] Qianwen Guan,[a] Lina Hua[a] and Junhua Luo*[a, b]

a. State Key Laboratory of Structure Chemistry, Fujian Institute of Research on the Structure of Matter, Chinese Academy of Sciences, Fuzhou 350002, P. R. China

b. College of Chemistry and Materials Science, Fujian Normal University, Fuzhou 350007, P. R. China

E-mail: jhluo@fjirsm.ac.cn.

Figures

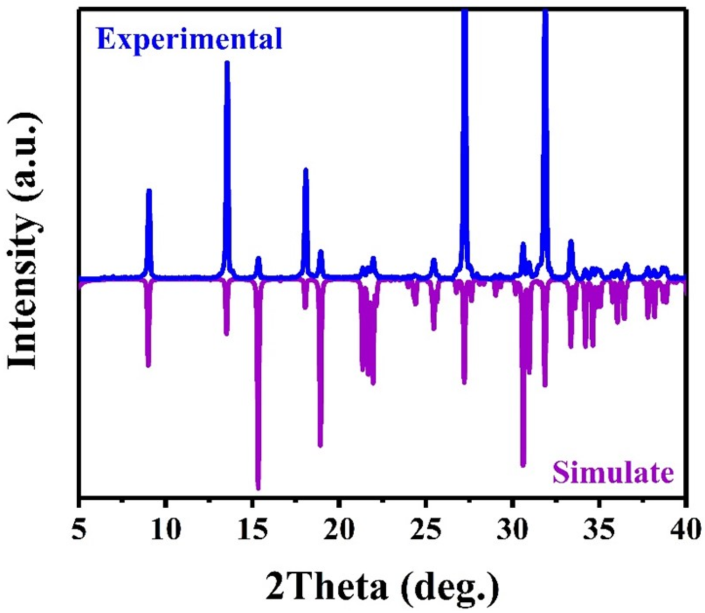

Figure S1. Experimental and calculated powder X-ray diffraction patterns of $(BA)_2CsPb_2Br_7$ at room temperature.

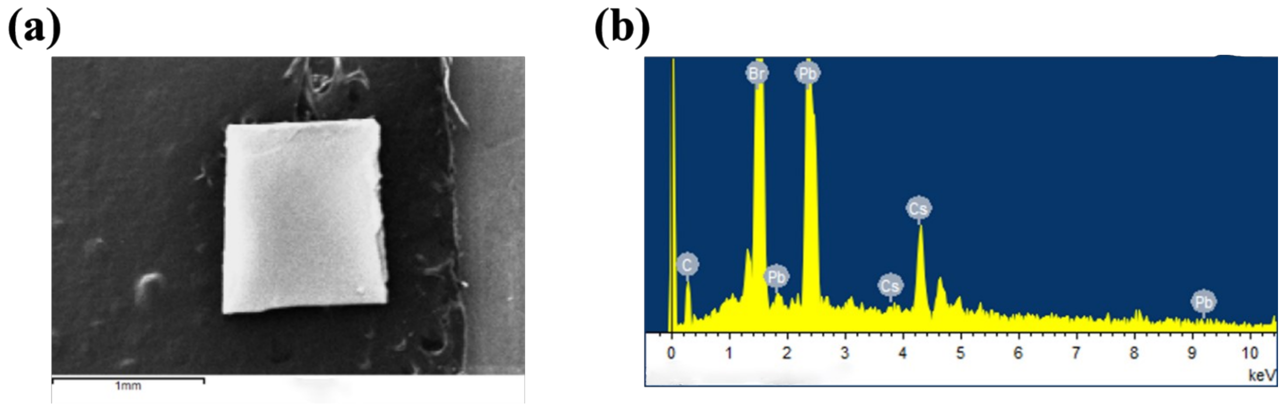

Figure S2. (a) Image and (b) EDS patterns of the $(BA)_2CsPb_2Br_7$ single crystal.

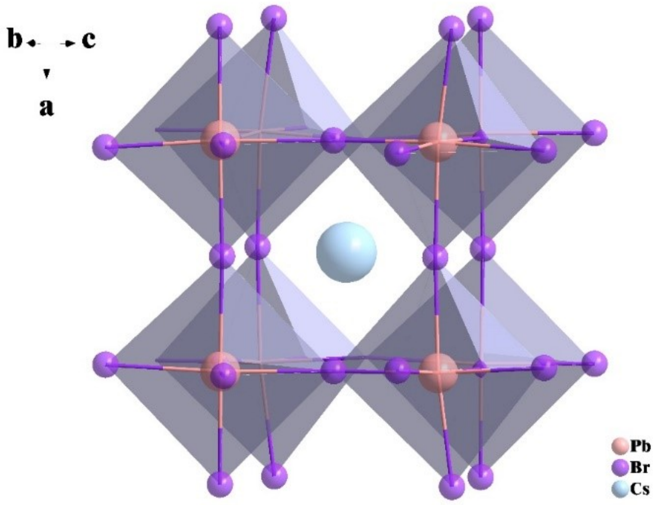

Figure S3. Crystal structures of cubic 3D perovskite $CsPbBr_3$.

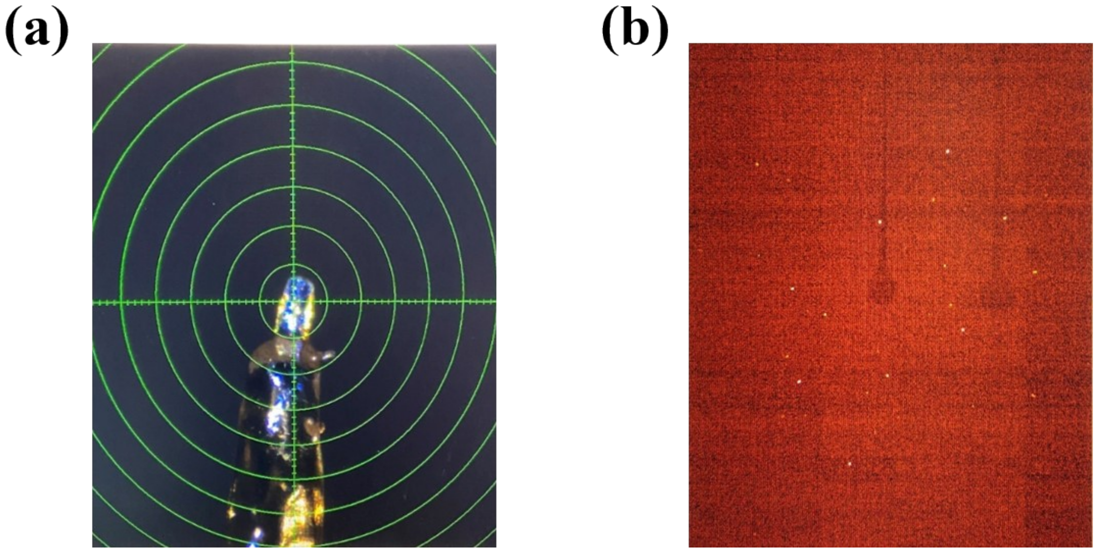

Figure S4. a) Image and b) SCXRD diffraction patterns of the $(BA)_2CsPb_2Br_7$ single crystal.

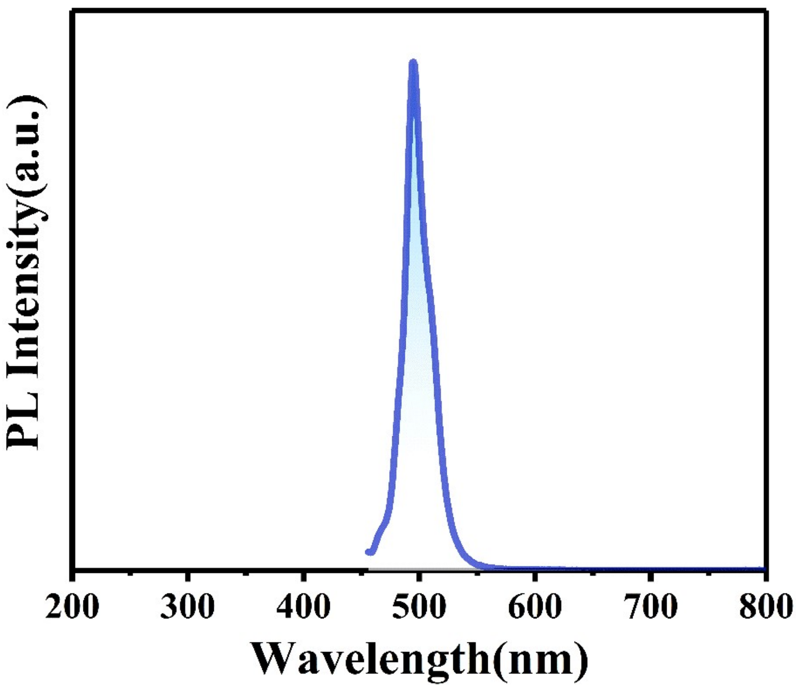

Figure S5. PL spectra of the $(BA)_2CsPb_2Br_7$.

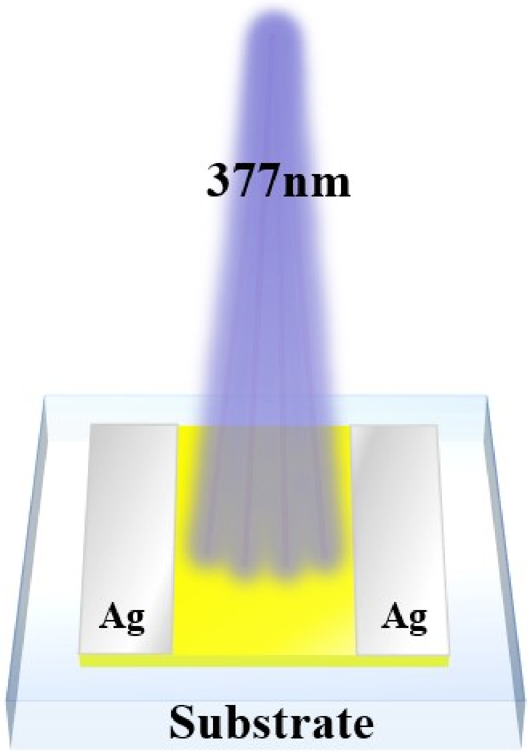

Figure S6. Device structure of the $(BA)_2CsPb_2Br_7$ crystal-based photodetector.

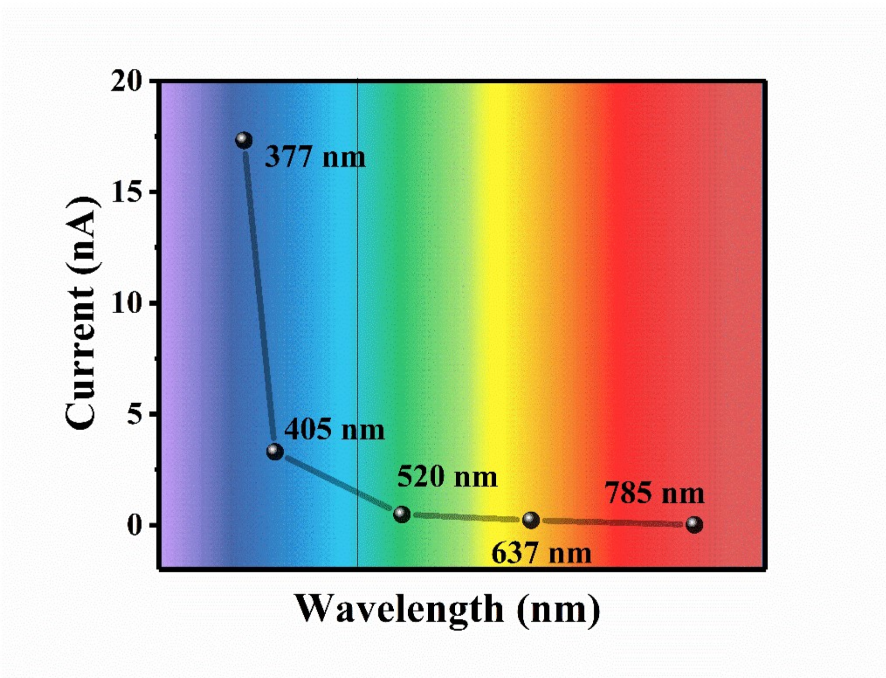

Figure S7. Wavelength-dependent photoresponse of $(BA)_2CsPb_2Br_7$.

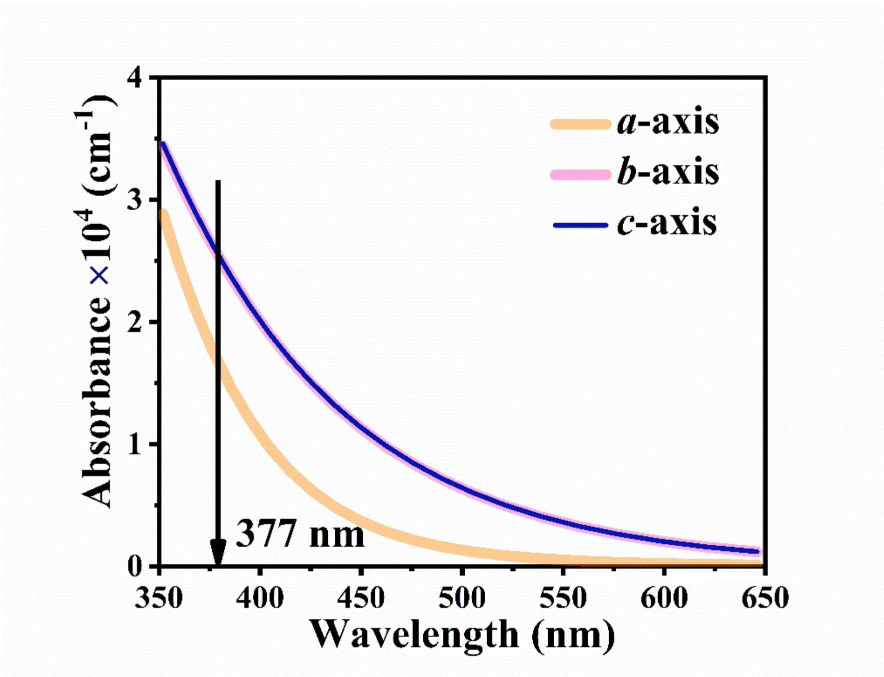

Figure S8. Strong anisotropy of optical absorbance along different axes at 377 nm for the crystal of the $(BA)_2CsPb_2Br_7$.

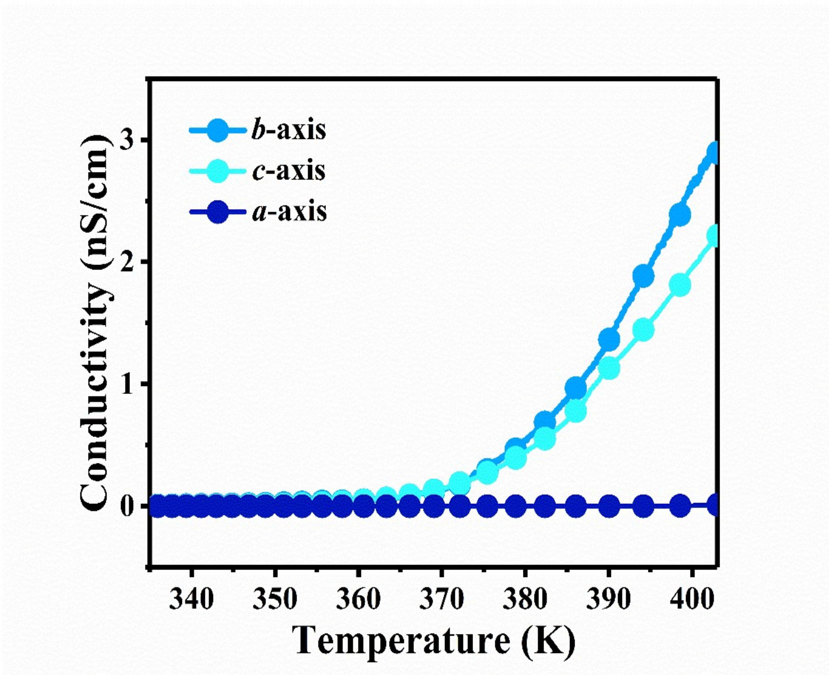

Figure S9. Anisotropic conductivity along different axes for the crystal of the $(BA)_2CsPb_2Br_7$.

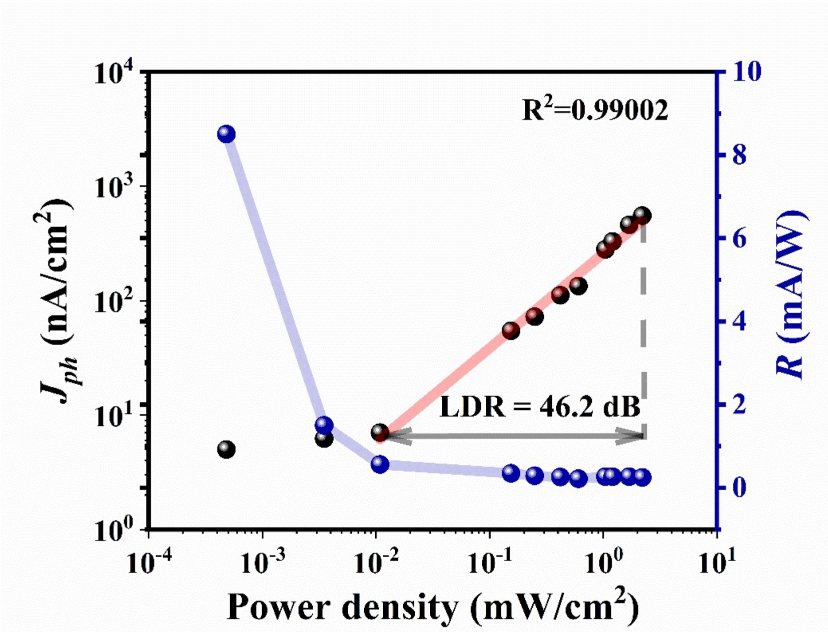

Figure S10. J_{ph} and R dependence on the light intensity of the device at the wavelength of 377nm under 10 V bias.

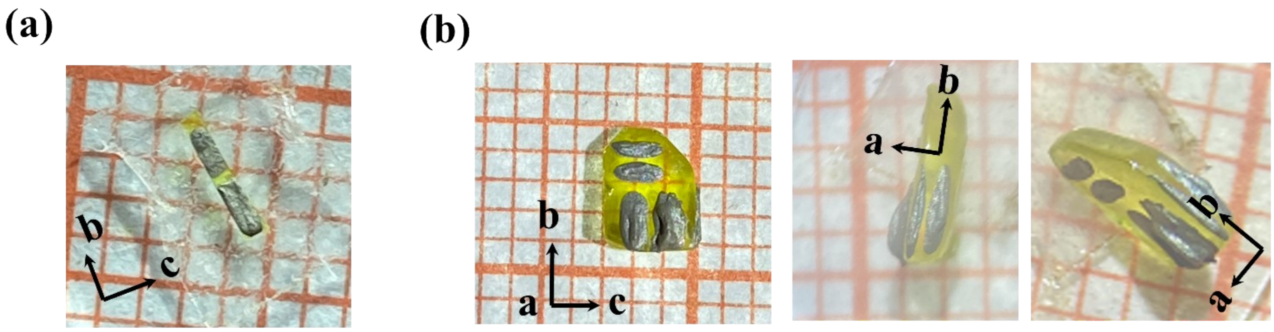

Figure S11. (a) The photograph of the planar-type device based on the $(BA)_2CsPb_2Br_7$ single crystal for ordinary photodetection tests. (b) The photographs of the planar-type device based on the $(BA)_2CsPb_2Br_7$ single crystal for anisotropic photodetection tests.

Table S1. Comparison of anisotropic properties of photodetectors using different materials.

Photodetector	Wavelength (nm)	Bias (V)	Photocurrent anisotropy ratio (Power density)	**Ref.**
$(C_6H_5C_2H_4NH_3)_2PbI_4$ SC	462	6	57.62 (-)	**1**
$(NH_4)_3Bi_2I_9$ SC	450	10	~2 （0.8 mW/cm²）	**2**

(n-propylammonium)(MA)$SbBr_5$ SC	405	10	35 (100 mW/cm^2)	**3**
(i-BA)$_2$CsPb_2Br_7 SC	425	10	~4 （22.4 mW/cm^2）	**4**
(s-BA)$_2$(MA)Pb_2I_7 SC	520	10	~10 (-)	**5**
(TRA)$_2$CsPb_2Br_7 SC	405	10	~10 (-)	**6**
(FPEA)$_2$$PbI_4$ SC	520	10	<10 (-)	**7**
$Cs_2[C(NH_2)_3]Pb_2Br_7$ SC	405	10	~10 (-)	**8**
(BA)$_2$CsPb_2Br_7 SC	377	10	25 (26 mW/cm^2)	**This work**

i-BA= isobutylamine; s-BA=sec-butylammonium; TRA=(carboxy)cyclohexylmethylammonium; FPEA= p-fluorophenethylammonium.

Table S2. Parameter comparison of UV photodetectors using different materials.

Photodetectors	Wavelength (nm)	Bias (V)	Detectivity (Jones)	Response time (rise/decay)	**Ref**
(BA)$_2$CsPb_2Br_7 SC	377	10	5.08×10^{11}	260 μs/430 μs	**This work**
$MAPbCl_3$ SC	365	15	6.07×10^{11}	130 ns/365 μs	**9**
$EA_4Pb_3Cl_{10}$ SC	266	0	3.06×10^{9}	0.8 s/0.22 s	**10**
$MAPbI_3/TiO_2$	350	1	2.5×10^{12}	2 s/1 s	**11**
$SnS_2/ZnO_{1-x}S_x$	365	-	5.1×10^{10}	49.51 ms/25.93 ms	**12**
Few-layers SnS	365	-	1.92×10^{8}	0.3 s/0.5 s	**13**
[(R)-MPA]$_2$$PbCl_4$/Si	266	10	1.2×10^{12}	500 μs/600 μs	**14**
(BPA)$_2$$PbBr_4$	377	0	~10^{7}	27 μs/30 μs	**15**
(PMA)$_2$$PbCl_4$ MMB	320	0	1.01×10^{11}	162 μs/226 μs	**16**

(R)-MPA=methylphenethylammonium; BPA= 3-bromopropylammonium; PMA= benzylammonium.

References

1 Y. C. Liu, H. C. Ye, Y. X. Zhang, K. Zhao, Z. Yang, Y. B. Yuan, H. D. Wu, G. T. Zhao, Z. P. Yang, J. Tang, Z. Xu and S. Z. Liu, Surface-Tension-Controlled Crystallization for High-Quality 2D Perovskite Single Crystals for Ultrahigh Photodetection, *Matter*, 2019, **1**, 465-480.

2 R. Zhuang, X. Wang, W. Ma, Y. Wu, X. Chen, L. Tang, H. Zhu, J. Liu, L. Wu, W. Zhou, X. Liu and Y. Yang, Highly sensitive X-ray detector made of layered perovskite-like $(NH_4)_3Bi_2I_9$ single crystal with anisotropic response, *Nat. Photonics*, 2019, **13**, 602.

3 W. Zhang, M. Hong and J. Luo, Centimeter-Sized Single Crystal of a One-Dimensional Lead-Free Mixed-Cation Perovskite Ferroelectric for Highly Polarization Sensitive Photodetection, *J. Am. Chem. Soc.*, 2021, **143**, 16758-16767.

4 B. Xiao, Q. Sun, F. Wang, S. Wang, B.-B. Zhang, J. Wang, W. Jie, P. Sellin and Y. Xu, Towards superior X-ray detection performance of two-dimensional halide perovskite crystals by adjusting the anisotropic transport behavior, *J. Mater. Chem. A*, 2021, **9**, 13209-13219.

5 X. Li, D. Li, Y. Peng, Y. Liu, J. Wang, L. Li, Y. Yao, X. Liu and J. Luo, Exploring a layered iodide perovskite crystal with centimetered dimension for extended spectral polarization-sensitive photodetection, *J. Mater. Chem. C*, 2021, **9**, 9499-9504.

6 Y. Liu, J. Wang, S. Han, X. Liu, M. Li, Z. Xu, W. Guo, M. Hong, J. Luo and Z. Sun, Multilayered 2D Cesium-Based Hybrid Perovskite with Strong Polarization Sensitivity: Dimensional Reduction of $CsPbBr_3$, *Chem. Eur. J.*, 2020, **26**, 3494-3498.

7 M. Li, S. Han, B. Teng, Y. Li, Y. Liu, X. Liu, J. Luo, M. Hong and Z. Sun, Minute-Scale Rapid Crystallization of a Highly Dichroic 2D Hybrid Perovskite Crystal toward Efficient Polarization-Sensitive Photodetector, *Adv. Opt. Mater.*, 2020, **8**, 2000149.

8 Q. Chen, Z. Wang, Y. Fan, Z. Li, S. Zhang, J. Luo and C. Ji, Polarization-sensitive photodetection in a two-dimensional interlayer-multiple-cation hybrid perovskite bulk single crystal, *J. Mater. Chem. C*, 2022, **10**, 5882-5886.

9 Z. Cheng, K. Liu, J. Yang, X. Chen, X. Xie, B. Li, Z. Zhang, L. Liu, C. Shan and D. Shen, High-Performance Planar-Type Ultraviolet Photodetector Based on High-Quality $CH_3NH_3PbCl_3$ Perovskite Single Crystals, *ACS Appl. Mater. Interfaces*, 2019, **11**, 34144-34150.

10 S. Wang, L. Li, W. Weng, C. Ji, X. Liu, Z. Sun, W. Lin, M. Hong and J. Luo, Trilayered Lead Chloride Perovskite Ferroelectric Affording Self-Powered Visible-Blind Ultraviolet Photodetection with Large Zero-Bias Photocurrent, *J. Am. Chem. Soc.*, 2020, **142**, 55-59.

11 Z. Zheng, F. Zhuge, Y. Wang, J. Zhang, L. Gan, X. Zhou, H. Li and T. Zhai, Decorating Perovskite Quantum Dots in TiO_2 Nanotubes Array for Broadband Response Photodetector, *Adv. Funct. Mater.*, 2017, **27**, 1703115.

12 J. C. Jiang, J. Y. Huang, Z. Z. Ye, S. C. Ruan and Y. J. Zeng, Self-Powered and Broadband Photodetector Based on $SnS_2/ZnO_{1-x}S_x$Heterojunction, *Adv. Mater. Interfaces*, 2020, **7**, 2000882.

13 W. Huang, Z. Xie, T. Fan, J. Li, Y. Wang, L. Wu, D. Ma, Z. Li, Y. Ge, Z. N. Huang, X. Dai, Y. Xiang, J. Li, X. Zhu and H. Zhang, Black-phosphorus-analogue tin monosulfide: an emerging optoelectronic two-dimensional material for high-performance photodetection with improved stability under ambient/harsh conditions, *J. Mater. Chem. C*, 2018, **6**, 9582-9593.

14 X. Zhang, W. Weng, L. Li, H. Wu, Y. Yao, Z. Wang, X. Liu, W. Lin and J. Luo, Heterogeneous Integration of Chiral Lead-Chloride Perovskite Crystals with Si Wafer for Boosted Circularly Polarized Light Detection in Solar-Blind Ultraviolet Region, *Small*, 2021, **17**, 2102884.

15 C. Ji, D. Dey, Y. Peng, X. Liu, L. Li and J. Luo, Ferroelectricity-Driven Self-Powered Ultraviolet Photodetection with Strong Polarization Sensitivity in a Two-Dimensional Halide Hybrid Perovskite, *Angew. Chem. Int. Ed.*, 2020, **59**, 18933-18937.

16 L. Guo, X. Liu, L. Gao, X. Wang, L. Zhao, W. Zhang, S. Wang, C. Pan and Z. Yang, Ferro-Pyro-Phototronic Effect in Monocrystalline 2D Ferroelectric Perovskite for High-Sensitive, Self-Powered, and Stable Ultraviolet Photodetector, *ACS nano*, 2022, **16**, 1280-1290.